Electronic Supplementary Information

Fluorescent Dye Nano-Assemblies by Thiol Attachment Directed to the Tips of Gold Nanorods for Effective Emission Enhancement

David Botequim,[a,b] Inês I. R. Silva,[a] Sofia G. Serra,[a] Eduardo P. Melo,[c] Duarte M. F. Prazeres,[b]* Sílvia M. B. Costa,[a] Pedro M. R. Paulo [a]*

a. Centro de Química Estrutural, Instituto Superior Técnico, Universidade de Lisboa, Av. Rovisco Pais 1, 1049-001 Lisboa, Portugal. E-mail: pedro.m.paulo@tecnico.ulisboa.pt
b. iBB-Institute for Bioengineering and Biosciences, Instituto Superior Técnico, Universidade de Lisboa, Av. Rovisco Pais 1, 1049-001 Lisboa, Portugal. E-mail: miguelprazeres@tecnico.ulisboa.pt
c. CCMAR - Centro de Ciências do Mar, Universidade do Algarve, Campus de Gambelas, 8005-139 Faro, Portugal

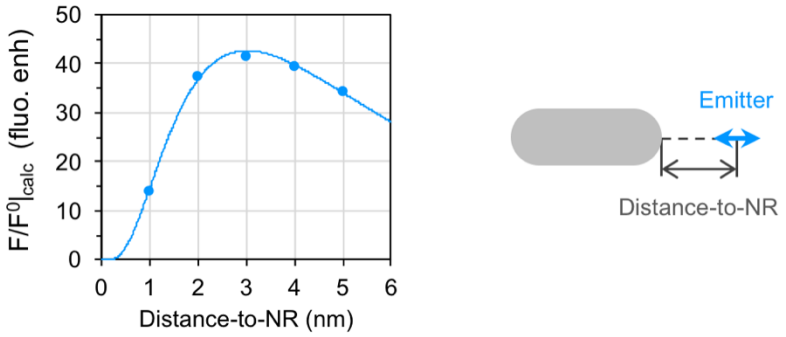

Fig. S1 Fluorescence enhancement factors, $F/F^0|_{calc}$, calculated from DDA simulations of an emitter with the photophysical properties of Atto-647N dye positioned at the tip of a gold nanorod with a size of 25 nm × 61 nm – see dye-particle configuration on the right-side scheme – for excitation and emission at 639 and 700 nm, respectively. The calculated enhancement factors show that the maximum enhancement effect for this particle configuration is about 40-fold emission increase at a distance of 3 to 4 nm away from the particle's surface.

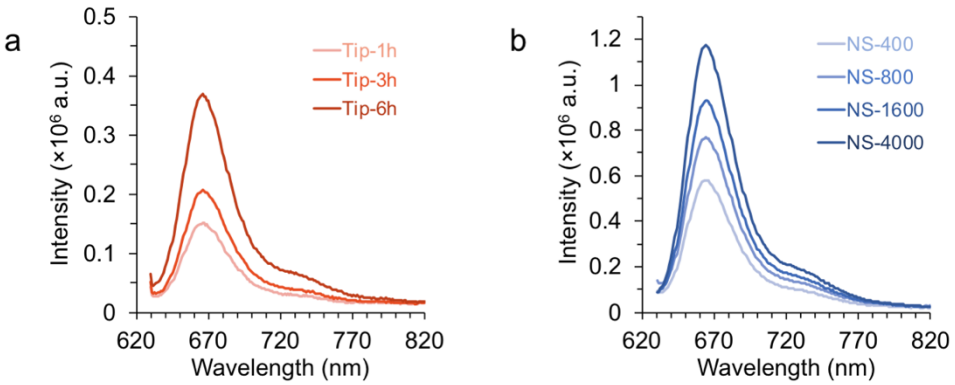

Fig. S2 Emission spectra of dye displaced from nano-assemblies used to quantify the amount of loaded DNA per particle: (a) tip-selective functionalized gold nanorod samples for several incubation times; (b) non-selective functionalized gold nanorod samples for various DNA loading ratios – excitation wavelength at 620 nm.

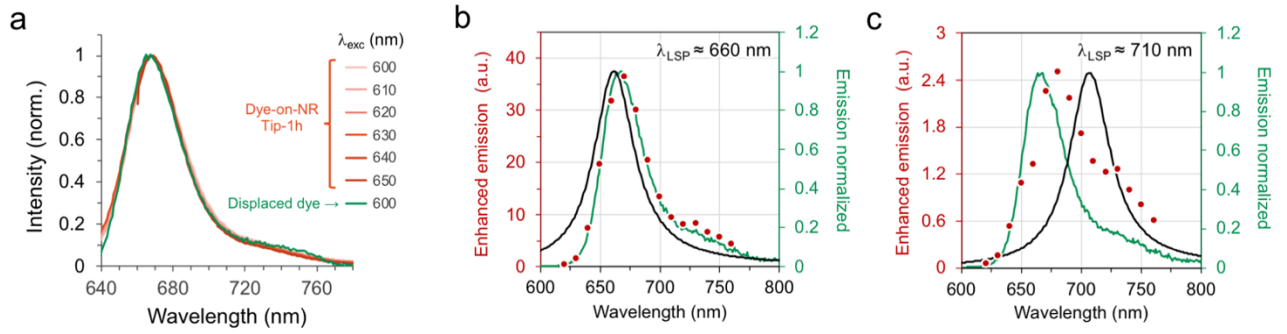

Fig. S3 (a) Normalized emission spectra of tip-functionalized gold nanorods (sample "Tip-1h") measured for several excitation wavelengths (red curves) showing a similar lineshape and comparison to the emission spectrum of the displaced dye in aqueous solution (green curve); (b,c) simulated spectra for the dye's enhanced emission (red dots) by a gold nanorod, in two illustrative cases: (b) good spectral overlap between the dye's emission (green curve) and the longitudinal surface plasmon band (black curve); or (c) large mismatch between them. These simulations suggest that a possible explanation for the apparent absence of spectral reshaping in the plasmon-coupled emission of our dye-particle assemblies could be due to a good spectral overlap between the dye's emission and the longitudinal surface plasmon band.

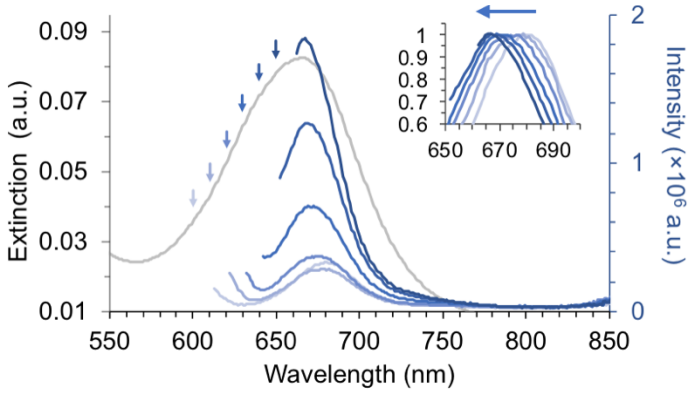

Fig. S4 Extinction spectrum of the non-selectively functionalized gold nanorods for "NS-4000" sample (grey curve) and emission spectra of the same sample for several excitation wavelengths (blue curves) indicated by the arrows over the extinction spectrum. The inset shows the change in the fluorescence spectrum close to its maximum, as excitation is selected at longer wavelengths (see arrow).

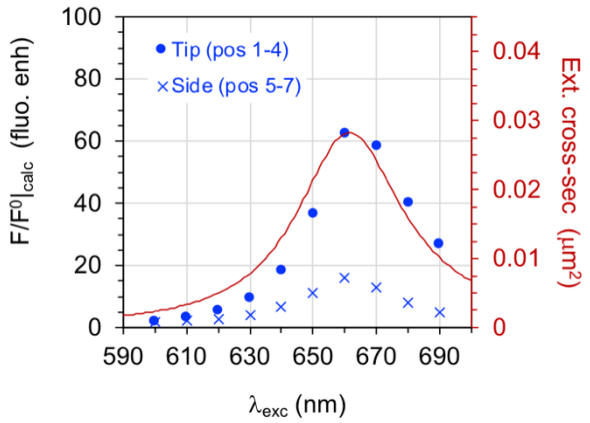

Fig. S5 Spectral dependence of the calculated enhancement factor ($F/F^0|_{calc}$) on the excitation wavelength for an average of the positions simulated at the tip and side regions (circles and crosses, respectively). The simulated emitter positions are shown in Fig. 4e of the main text. These results consider an average dipole orientation of the emitter. The calculated extinction spectrum for the simulated nanorod is depicted in red – axis on the right-side.

Analysis of autocorrelation function curves from single-particle fluorescence emission

Further information from the intensity traces shown in Fig. 5 of the main text was obtained from their autocorrelation function (ACF). The ACF curves show two relaxation components that were attributed to rotational and translational diffusion motions of the dye-particle nano-assemblies in colloidal suspension,[S1]

$$G(\tau) - 1 = \left(1 - A_s e^{-\tau/\tau_\perp}\right) \times \frac{1}{N}\left(1 + \frac{\tau}{\tau_w}\right)^{-1}\left(1 + \frac{\tau}{\kappa^2 \cdot \tau_w}\right)^{-1/2} \quad \text{(S1)}$$

The relaxation times for the short component were used to calculate the rotational diffusion coefficient of the dye-particle nano-assemblies from: $\tau_\perp = 1/6D_r^\perp$. The values of $\tau_\perp$ fitted from the ACF curves of samples "Tip-1h" and "NS-4000" (shown in Fig. 5e,f of the main text) were 80 and 49 μs, and these correspond to $D_r^\perp$ values of 2.1 and 3.4 ms^{-1}, respectively (Table S1). For comparison purposes, the rotational diffusion coefficient for these nano-objects was theoretically estimated using a modified version of Einstein–Smoluchowski relation for a rod-like particle geometry,[S2]

$$D_r^\perp = 3\frac{kT(\ln p + C_r^\perp)}{\pi\,\eta\,L^3} \quad \text{(S2)}$$

where p is the ratio between the rod's length L and diameter d, and $C_r^\perp$ is an end-effect term that depends on the aspect ratio, $C_r^\perp = -0.662 + 0.917/p - 0.050/p^2$. The dimensions of gold nanorods were 25 nm × 71 nm, but were increased by the length of the DNA which is approximately 4 nm. This yielded an estimate of 4.8 ms^{-1} for the rotational diffusion coefficient that compares well with the experimental values fitted from ACF curves. Similarly, the long relaxation times of 7.7 and 5.6 ms for samples "Tip-1h" and "NS4000" were used to calculate the respective translational diffusion constants ($\tau_w = w_{xy}^2/4D_t$) yielding values of of 6.2 and 7.8 μm^2/s for these samples. The latter values compare well to the theoretical estimate of 8.0 μm^2/s obtained for a rod-like object with the size previously assumed for these nano-assemblies,[S2]

$$D_t = \frac{kT(\ln p + C_t)}{3\pi\,\eta\,L} \quad \text{(S3)}$$

where p is again the ratio between the rod's length L and diameter d, and C_t is an end-effect term that depends on the aspect ratio, $C_t = 0.312 + 0.565/p - 0.100/p^2$. The ACF curves of the control systems are quite different (results not shown), because these display a single relaxation component with longer decay times due to the translational diffusion of dye-labelled oligonucleotides either bound to CTAB micelles ("Control 1"), or free in solution ("Control 2"), which are both objects much smaller than gold nanorods.

Table S1 Values of the short and long relaxation times ($\tau_\perp$ an τ_w) fitted from ACF curves of samples of dye-partlicle nano-assemblies studied, and respective rotational and translational diffusion coefficients ($D_r^\perp$ and D_t) obtained from experimental data or theoretically estimated.

		$D_r^\perp$ /ms^{-1}			D_t /μm^{2}s^{-1}	
Sample	$\tau_\perp$ /μs	exp.	calc.	τ_w /ms	exp.	calc.
Tip-1h	80	2.1	4.8	7.7	6.2	8.0
Tip-3h	57	2.9		5.7	8.2	
Tip-6h	96	1.7		6.7	6.7	
NS-400	52	3.2	4.8	5.1	8.3	8.0
NS-800	54	3.1		6.3	6.7	
NS-1600	51	3.3		5.4	8.0	
NS-4000	49	3.4		5.6	7.8	

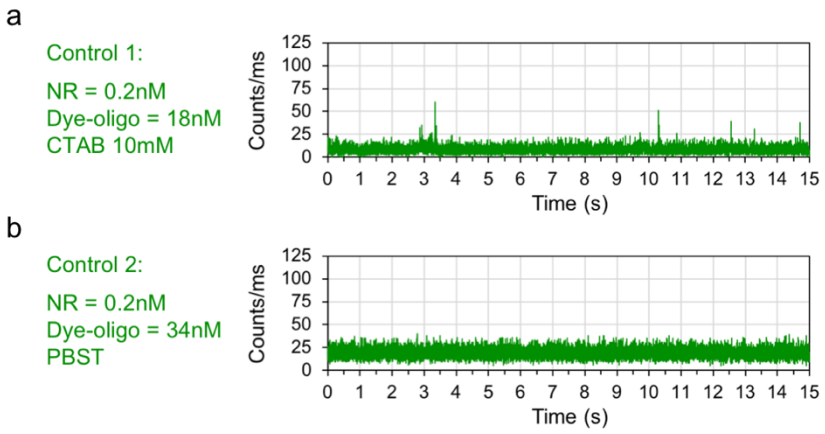

Fig. S6 Examples of intensity time traces of two control systems that do not show intense fluorescence bursts when the same amounts of the components present in samples "Tip-6h" and "NS-4000", respectively, are simply mixed together in: (a) aqueous CTAB; or (b) PBST buffer (*i.e.* without performing the functionalization protocols) – these intensity traces were measured for a much higher excitation power, 0.44 kW/cm^2, than those presented in Fig. 5 of the main text.

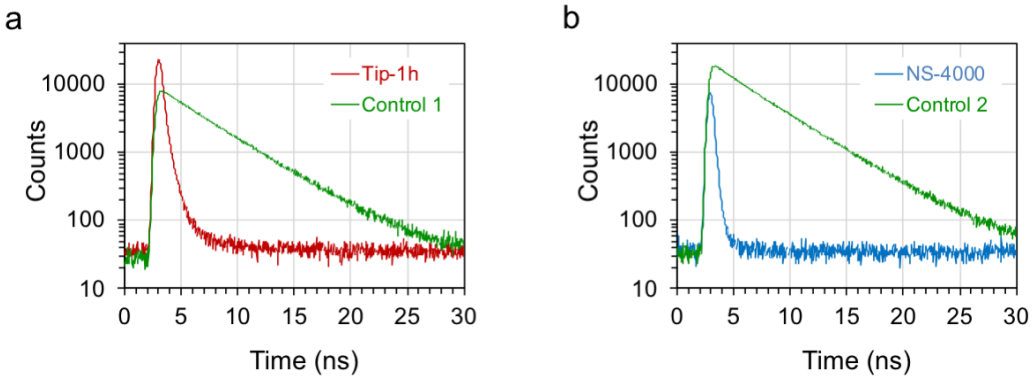

Fig. S7 Fluorescence decays of dye-particle nano-assemblies in colloidal suspension of: (a) tip-functionalized gold nanorods (sample "Tip-1h") and its control sample and (b) non-selectively functionalized gold nanorods (sample "NS-4000") and its control sample – control samples are described in Fig. S6. All measurements were performed in a time-resolved fluorescence microscope with picosecond diode laser excitation at 639 nm with a power of 4.4×10^{-3} kW/cm^2 for dye-particle samples, or a power of 0.44 kW/cm^2 for control systems, and for emission selected with a bandpass filter centered at 695 nm with a transmission window of 55 nm.

Cell internalization assays

Mouse neuroblastoma N2a cells genetically modified to express stably a construct of the prion protein (PrP) fused to the yellow fluorescent protein (YFP) GPI-anchored (glycosylphosphatidylinositol) for labelling the cell membrane were used in the internalization assays.[53] The genetically modified N2a cell line was cultured at 37 °C under 5% CO_2 in DMEM supplemented with 10% FBS, 100 µg/mL streptomycin and 100 U/mL penicillin (Invitrogen, USA) and incubated in the presence of a sub-nanomolar concentration of NS-functionalized gold nanorods. Cellular uptake was imaged 24 hours after incubation with nanorods and again two days later (after replacement of culture medium) by fluorescence imaging in a laser scanning confocal microscope equipped with a 63× plan-apochromatic 1.4 NA oil immersion objective and sub-diffraction spatial resolution (Carl Zeiss Axio Observer Z1 mounted LSM710 confocal microscope). Three detection channels were used for excitation at 405, 514 and 633 nm, respectively, for detection of nuclei stained with Hoechst 33342 dye, cell membranes labelled with PrP-YFP-GPI-anchor fusion protein, and dye-particle nano-assemblies labelled with Atto-647N dye.

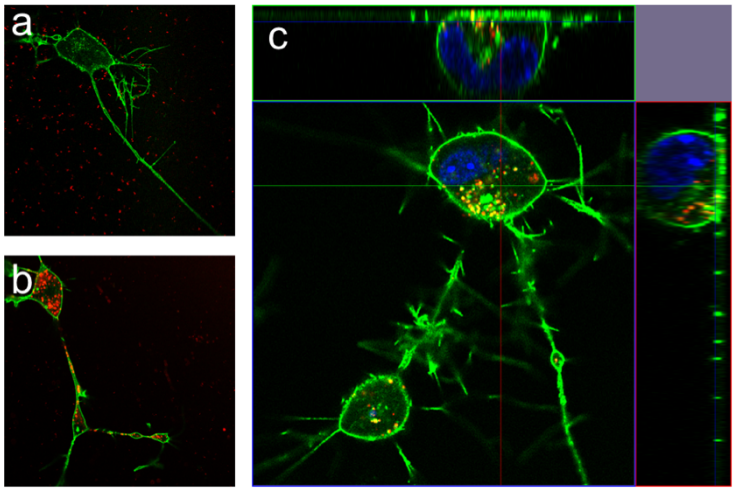

Fig. S8 Cell internalization of fluorescent dye-particle nano-assemblies by live neuroblastoma N2a cells expressing stably a fusion of the prion protein-YFP-GPI-anchored to label the plasma membrane: (a) confocal microscopy image of N2a cells immediately after the addition ($t = 0$) of dye-particles showing their location outside the cell; (b) after an incubation time of 24 hours showing that dye-particles have been internalized, and; (c) high-resolution fluorescence image after 48 hours of incubation time showing by orthogonal projection that dye-particle assemblies are inside the cell volume.

Table S2 Comparison of literature reports on dye-particle assemblies based on gold nanorods that display fluorescence enhancement. The examples selected illustrate the diversity of surface chemistries used for dye assembly onto gold nanorods, although most approaches are not tip-selective. The enhancement factors presented on this table are the top values reported on each study.

Reference	λ_{LSP} length x width	Dye assembly onto gold NRs	Tip	Purpose or application	Enhanc. factor	FOM [a]
S4	804 nm (46 x 11)	Human Serum Albumin with covalently linked IR800 dye	No	Fundamental study	9	0.9
S5	647 nm (89 x 42)	Silica shell with entrapped oxazine 725 dye	No	Fundamental study	37 [b]	5.2
S6	800 nm (35 x 9.3)	Poly(styrene-alt-maleic acid) with non-covalently attached indocyanine green	No	Photodynamic therapy, hyperthermia and near-infrared optical imaging	1.3	0.034
S7	850 nm (50 x 12)	CTAB bilayer with electrostatically adsorved chlorin e6	No	Fluorescence detection and photodynamic therapy	3	0.54
S8	776 nm (43 x 12) [c]	Silica shell with covalently linked IRDye	No	Fundamental study	10	0.7
S9	843 nm (54 x 13)	Silica shell with adsorbed doxorubicin dye	No	Fundamental study	2.9	0.26
S10	820 nm (85 x 20)	Silica shell with covalently linked porphyrin, T790	No	Two-photon imaging and photodynamic therapy	2.1	0.32
S11	668 nm (47 x 19)	Silica shell with covalently linked phthalocyanine, AlC4Pc	No	Co-enhancement of fluorescence and singlet oxygen generation	7	2.8
S12	654 nm (49 x 21)	Silica shell with covalently linked porphyrin, TCPP	No	Sensor for detection of pyrophosphate in aqueous solution	4.5	0.45
S13	664 nm (50 x 25)	Oligo dsDNA spacer with 45-bp labelled with Quasar 670	Yes [d]	Array biochip for ultrasensitive DNA analysis	< 2	< 0.6
S14	615 nm (40 × 17)	Polyelectrolytes (PSS/PDADMAC) with electrostatically adsorved CdSe/CdZnS QDs	No	Fundamental study	10.8	2.2
Our work	662 nm (71 x 25)	Oligo dsDNA spacer with 10-bp labelled with Atto-647N	Yes	Fundamental study	17	11

[a] FOM$= \mathrm{Enh.\,factor} \times \phi^0$ is a figure-of-merit defined in Ref. S15 for comparison of enhancement effects between dyes of strikingly different quantum yield, ϕ^0.

[b] In this work, the enhancement effect was evaluated from a single-particle type of measurement, while other examples in the table are from ensemble measurements.

[c] The nanorod size was assessed from TEM images reported in Ref. S8.

[d] In this work, the dye molecules are assembled onto surface-immobilized nanorods, instead of an attachment in colloidal dispersion that is used in the remaining examples.

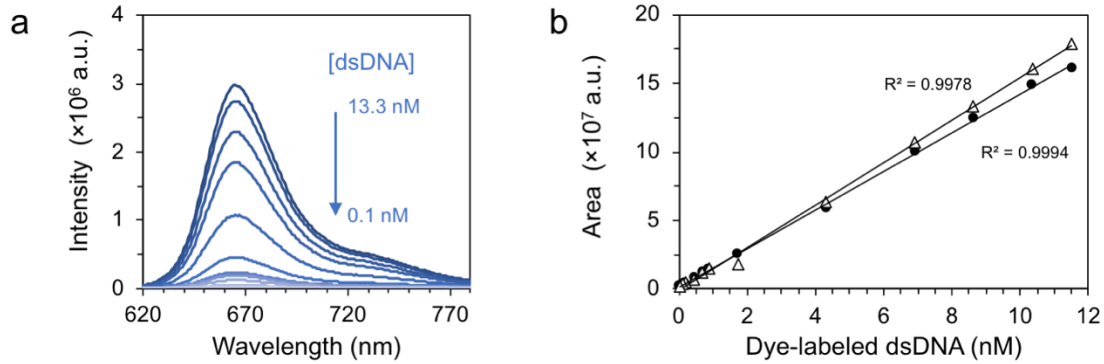

Fig. S9 Additional information for evaluating the number of dye-labelled oligonucleotides attached per gold nanorod: (a) emission spectra of dye-labelled oligonucleotides with known concentrations in the presence of 2-mercaptoethanol (20 mM) obtained for an excitation wavelength of 600 nm; (b) working curve for the determination of dye-labelled oligonucleotide concentration in the displacement assays: here represented as the integrated emission spectra (area) for solutions of known concentrations of dye-labelled oligonucleotides in PBST buffer (closed circles) and aqueous CTAB (open triangles) both in the presence of 2-mercaptoethanol (20 mM).

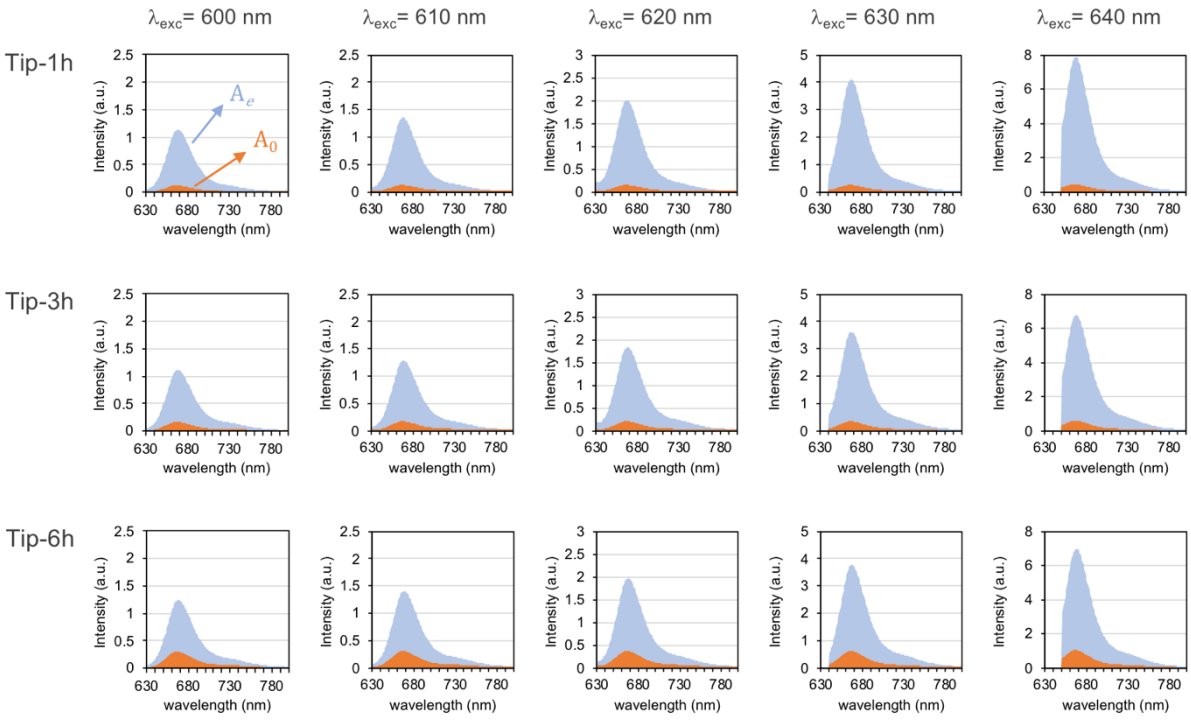

Fig. S10 Evaluation of fluorescence enhancement in tip-functionalized gold nanorods from comparison of the emission spectra of dye-particle nano-assemblies (light blue shaded areas) with that of the same sample after displacement of dye-labelled oligonucleotides into solution (orange shaded areas) - the enhancement factor is determined from the ratio of the respective areas, Fluo. enh $= A_e/A_0$. The data is displayed according to the excitation wavelength (λ_{exc}), as indicated at top of each column, and the sample incubation time used for DNA loading (1, 3 and 6 hours), as indicated at the beginning of each line.

Table S3 Fluorescence enhancement factors determined from data shown in Fig. S10.

Enhancement factor:	λ_{exc} /nm					
	600	610	620	630	640	650
Tip-1h	7.2	8.5	10.6	13.4	15.5	17.0
Tip-3h	5.7	6.4	7.7	9.3	10.4	11.2
Tip-6h	3.7	4.1	4.8	5.6	6.2	6.6

Table S4 Values of zeta potential determined for gold nanorod samples. The surface charge of dye-particle nano-assemblies was assessed in a Zetasizer Nano ZS from Malvern Instruments Ltd (Malvern, UK), using the Zetasizer Software, version 7.10. The zeta potential of all samples was recorded at 25 °C and 6 measurements were made to guarantee data reproducibility. The zeta potential values for NS-functionalized samples were measured in sub-nanomolar concentrations in water and are negative, because the CTAB bilayer in the "unmodified" nanorod sample is first replaced with thiolated PEG ("mPEG only" sample) and then dye-labeled oligonucleotides are inserted (in various loading ratios), which are negatively charged. For tip-functionalized gold nanorods, a previous dilution to sub-nanomolar concentrations was performed with aqueous CTAB (10 mM). The values of zeta potential determined for these samples probably reflect the micellar composition of the medium.

Gold nanorod samples	ζ-potential (mV)
unmodified[(a)]	31 ± 5
mPEG only	-15 ± 2
NS-400	-22 ± 3
NS-800	-19 ± 2
NS-1600	-26 ± 1
NS-4000	-29 ± 2
unmodified[(b)]	53 ± 4
Tip-1h	69 ± 6
Tip-3h	58 ± 4
Tip-6h	58 ± 3

[(a)] Original gold nanorods in aqueous CTAB 1 mM or [(b)] 10 mM.

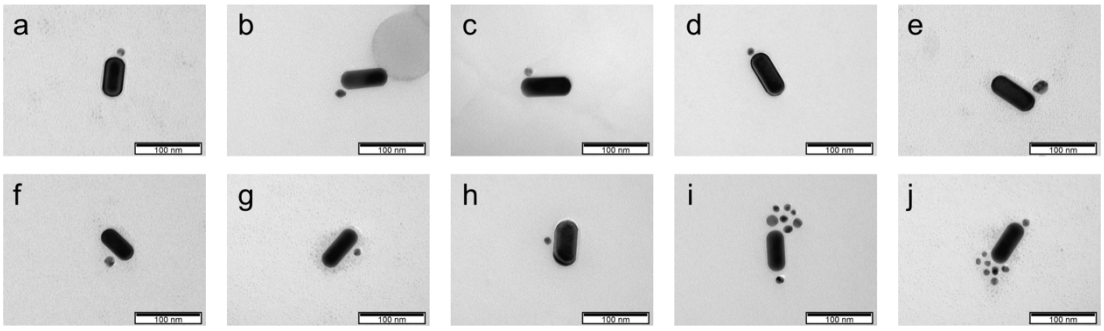

Fig. S11 Validation of tip-selective functionalization by promoting hybridization between tip-functionalized gold nanorods with a thiolated ssDNA of 24 nts and gold nanospheres coated with the complementary sequence: 5'-CAG CCC CAT AGA TTG CTC CGA AAA-3'-SH. Examples of TEM images showing: (a-e) tip assembly, and (f-h) side assembly. From a total of 39 nanorods evaluated with 68 nanospheres assembled, the ratio of 40:28 was obtained for a tip:side classification, showing that the majority of assembled nanospheres are at the nanorods' tips. A non-negligible fraction of side-assembled particles has also been reported in previous studies from the literature.[S16-S18] In our work, it is plausible that some additional side assembly could have been promoted by electrostatic adsorption between positively charged sides of nanorods and negatively charged nanospheres. Besides tip-selective assembly, it was also noticed self-aggregation of nanospheres (images i and j) even after washing by two cycles of centrifugation and resuspension in aqueous CTAB solution.

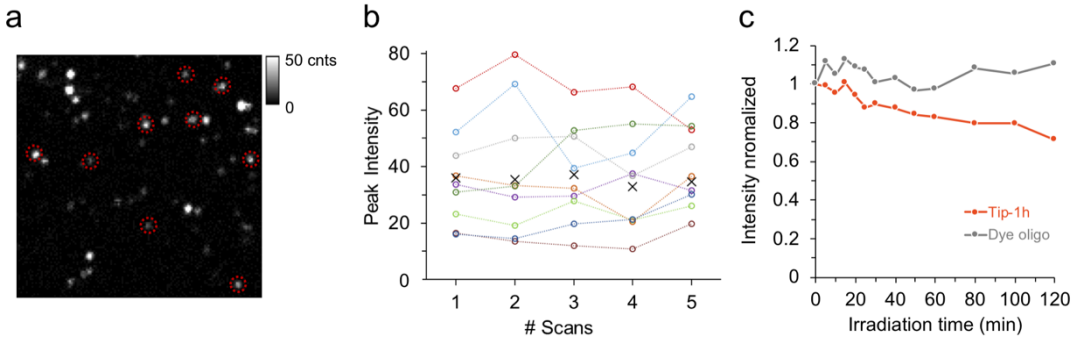

Fig. S12 Evaluation of photo-damage on tip-functionalized gold nanorods by scanning successive images with excitation at 639 nm using a power of 0.044 kW/cm^2: (a) example of an image showing 9 selected particles (red dashed circles), and (b) evolution of peak intensity from PSF fitting (see Fig. 6 of the main text) for those selected particles (open symbols). For this assay, the particles have been covalently immobilized on a glass surface modified with (3-mercaptopropyl) trimethoxysilane and during image scans, the particles are immersed in pure water. The emission intensity from selected particles is preserved after 5 consecutive scans with minimal fatigue effects. This feature is more evident in the average emission from a larger sample of 47 particles (black crosses) that is free from signal fluctuations inherent to single particle measurements; (c) photobleaching effect on tip-functionalized gold nanorods was also evaluated from a conventional irradiation assay in a cuvette using a mercury lamp of 250 W and monitoring the emission intensity of a colloidal dispersion of dye-particle assemblies ("Tip-1h"). It was observed a decrease of about 30% after an accumulated irradiation time of 2 hours (red symbols). On the other hand, the same amount of free dye shows a negligible photobleaching effect (grey symbols). Literature reports on single-molecule fluorescence studies have suggested an opposite effect, in which plasmon-coupled emission could extend the number of detected photons from single dye molecules and, thus, results in improved dye photostability.[S19,S20]

References

S1 M.P. Busson, B. Rolly, B. Stout, N. Bonod, J. Wenger and S. Bidault, *Angew. Chem. Int. Ed.*, 2012, **51**, 11083-11087.
S2 A. Ortega and J. García de la Torre, *J. Chem. Phys.*, 2003, **119**, 9914-9919.
S3 E. Tavares, J. A. Macedo, P. M. R. Paulo, C. Tavares, C. Lopes and E. P. Melo, *Biochim. Biophys. Acta*, 2014, **1842**, 981-991.
S4 R. Bardhan, N. K. Grady, J. R. Cole, A. Joshi and N. J. Halas, *ACS Nano*, 2009, **3**, 744-752.
S5 T. Ming, L. Zhao, Z. Yang, H. Chen, L. Sun, J. Wang and C. Yan, *Nano Lett.*, 2009, **9**, 3896-3903.
S6 W.-S. Kuo, C.-N. Chang, Y.-T. Chang, M.-H. Yang, Y.-H. Chien, S.-J. Chen and C.-S. Yeh, *Angew. Chem. Int. Ed.*, 2010, **49**, 2711-2715.
S7 X. Huang, X.-J. Tian, W.-l. Yang, B. Ehrenberg and J.-Y. Chen, *Phys. Chem. Chem. Phys.*, 2013, **15**, 15727-15733.
S8 N. S. Abadeer, M. R. Brennan, W. L. Wilson and C. J. Murphy, *ACS Nano*, 2014, **8**, 8392-8406.
S9 X. Tian, J. Guo, Y. Tian, H. Tang and W. Yang, *RSC Adv.*, 2014, **4**, 9343-9348.
S10 T. Zhao, K. Yu, L. Li, T. Zhang, Z. Guan, N. Gao, P. Yuan, S. Li, S. Q. Yao, Q.-H. Xu and G. Q. Xu, *ACS Appl. Mater. Interfaces*, 2014, **6**, 2700-2708.
S11 X. Ke, D. Wang, C. Chen, A. Yang, Y. Han, L. Ren, D. Li and H. Wang, *Nanoscale Res. Lett.*, 2014, **9**, 666-8.
S12 L. Wang, Q. Song, Q. Liu, D. He and J. Ouyang, *Adv. Funct. Mater.*, 2015, **25**, 7017-7027.
S13 Z. Mei and L. Tang, *Anal. Chem.*, 2017, **89**, 633-639.
S14 L. Trotsiuk, A. Muravitskaya, O. Kulakovich, D. Guzatov, A. Ramanenka, Y. Kelestemur, H. V. Demir and S. Gaponenko *Nanotechnology* 2020, **31**, 105201-10.
S15 D. Punj, R. Regmi, A. Devilez, R. Plauchu, S. B. Moparthi, B. Stout, N. Bonod, H. Rigneault and J. Wenger, *ACS Photonics*, 2015, **2**, 1099-1107.
S16 L. Xu, H. Kuang, C. Xu, W. Ma, L. Wang and N. A. Kotov *J. Am. Chem. Soc.*, 2012, **134**, 1699-1709.
S17 P. Zijlstra, P. M. R. Paulo and M. Orrit, *Nat. Nanotechnol.*, 2012, **7**, 379-382.
S18 G. Wang, Y. Akiyama, N. Kanayama, T. Takarada and M. Maeda, *Small*, 2017, **13**, 1702137-8.
S19 J. V. Pellegrotti, G. P. Acuna, A. Puchkova, P. Holzmeister, A. Gietl, B. Lalkens, F. D. Stefani and P. Tinnefeld, *Nano Lett.*, 2014, **14**, 2831-2836.
S20 L. Grabenhorst, K. Trofymchuk, F. Steiner, V. Glembockyte and P. Tinnefeld, *Methods Appl. Fluoresc.*, 2020, **8**, 02400.